EUROPEAN ORGANIZATION FOR NUCLEAR RESEARCH

CERN-PH-EP/2005-035
15th July 2005

Colour reconnection in $e^+e^- \to W^+W^-$ at $\sqrt{s} = 189$–209 GeV

The OPAL Collaboration

Abstract

The effects of the final state interaction phenomenon known as colour reconnection are investigated at centre-of-mass energies in the range $\sqrt{s} \simeq 189$–209 GeV using the OPAL detector at LEP. Colour reconnection is expected to affect observables based on charged particles in hadronic decays of W^+W^-. Measurements of inclusive charged particle multiplicities, and of their angular distribution with respect to the four jet axes of the events, are used to test models of colour reconnection. The data are found to exclude extreme scenarios of the Sjöstrand-Khoze Type I (SK-I) model and are compatible with other models, both with and without colour reconnection effects. In the context of the SK-I model, the best agreement with data is obtained for a reconnection probability of 37%. Assuming no colour reconnection, the charged particle multiplicity in hadronically decaying W bosons is measured to be $\langle n_{\mathrm{ch}}^{\mathrm{qq}} \rangle = 19.38 \pm 0.05(\mathrm{stat.}) \pm 0.08(\mathrm{syst.})$.

(Sbmitted to Eur. Phys. J. C)

The OPAL Collaboration

G. Abbiendi[2], C. Ainsley[5], P.F. Åkesson[3,y], G. Alexander[22], G. Anagnostou[1], K.J. Anderson[9], S. Asai[23], D. Axen[27], I. Bailey[26], E. Barberio[8,p], T. Barillari[32], R.J. Barlow[16], R.J. Batley[5], P. Bechtle[25], T. Behnke[25], K.W. Bell[20], P.J. Bell[1], G. Bella[22], A. Bellerive[6], G. Benelli[4], S. Bethke[32], O. Biebel[31], O. Boeriu[10], P. Bock[11], M. Boutemeur[31], S. Braibant[2], R.M. Brown[20], H.J. Burckhart[8], S. Campana[4], P. Capiluppi[2], R.K. Carnegie[6], A.A. Carter[13], J.R. Carter[5], C.Y. Chang[17], D.G. Charlton[1], C. Ciocca[2], A. Csilling[29], M. Cuffiani[2], S. Dado[21], A. De Roeck[8], E.A. De Wolf[8,s], K. Desch[25], B. Dienes[30], J. Dubbert[31], E. Duchovni[24], G. Duckeck[31], I.P. Duerdoth[16], E. Etzion[22], F. Fabbri[2], P. Ferrari[8], F. Fiedler[31], I. Fleck[10], M. Ford[16], A. Frey[8], P. Gagnon[12], J.W. Gary[4], C. Geich-Gimbel[3], G. Giacomelli[2], P. Giacomelli[2], M. Giunta[4], J. Goldberg[21], E. Gross[24], J. Grunhaus[22], M. Gruwé[8], P.O. Günther[3], A. Gupta[9], C. Hajdu[29], M. Hamann[25], G.G. Hanson[4], A. Harel[21], M. Hauschild[8], C.M. Hawkes[1], R. Hawkings[8], R.J. Hemingway[6], G. Herten[10], R.D. Heuer[25], J.C. Hill[5], D. Horváth[29,c], P. Igo-Kemenes[11], K. Ishii[23], H. Jeremie[18], P. Jovanovic[1], T.R. Junk[6,i], J. Kanzaki[23,u], D. Karlen[26], K. Kawagoe[23], T. Kawamoto[23], R.K. Keeler[26], R.G. Kellogg[17], B.W. Kennedy[20], S. Kluth[32], T. Kobayashi[23], M. Kobel[3], S. Komamiya[23], T. Krämer[25], A. Krasznahorkay[30,e], P. Krieger[6,l], J. von Krogh[11], T. Kuhl[25], M. Kupper[24], G.D. Lafferty[16], H. Landsman[21], D. Lanske[14], D. Lellouch[24], J. Letts[o], L. Levinson[24], J. Lillich[10], S.L. Lloyd[13], F.K. Loebinger[16], J. Lu[27,w], A. Ludwig[3], J. Ludwig[10], W. Mader[3,b], S. Marcellini[2], A.J. Martin[13], T. Mashimo[23], P. Mättig[m], J. McKenna[27], R.A. McPherson[26], F. Meijers[8], W. Menges[25], F.S. Merritt[9], H. Mes[6,a], N. Meyer[25], A. Michelini[2], S. Mihara[23], G. Mikenberg[24], D.J. Miller[15], W. Mohr[10], T. Mori[23], A. Mutter[10], K. Nagai[13], I. Nakamura[23,v], H. Nanjo[23], H.A. Neal[33], R. Nisius[32], S.W. O'Neale[1,*], A. Oh[8], M.J. Oreglia[9], S. Orito[23,*], C. Pahl[32], G. Pásztor[4,g], J.R. Pater[16], J.E. Pilcher[9], J. Pinfold[28], D.E. Plane[8], O. Pooth[14], M. Przybycień[8,n], A. Quadt[3], K. Rabbertz[8,r], C. Rembser[8], P. Renkel[24], J.M. Roney[26], A.M. Rossi[2], Y. Rozen[21], K. Runge[10], K. Sachs[6], T. Saeki[23], E.K.G. Sarkisyan[8,j], A.D. Schaile[31], O. Schaile[31], P. Scharff-Hansen[8], J. Schieck[32], T. Schörner-Sadenius[8,z], M. Schröder[8], M. Schumacher[3], R. Seuster[14,f], T.G. Shears[8,h], B.C. Shen[4], P. Sherwood[15], A. Skuja[17], A.M. Smith[8], R. Sobie[26], S. Söldner-Rembold[16], F. Spano[9,y], A. Stahl[3,x], D. Strom[19], R. Ströhmer[31], S. Tarem[21], M. Tasevsky[8,d], R. Teuscher[9], M.A. Thomson[5], E. Torrence[19], D. Toya[23], P. Tran[4], I. Trigger[8], Z. Trócsányi[30,e], E. Tsur[22], M.F. Turner-Watson[1], I. Ueda[23], B. Ujvári[30,e], C.F. Vollmer[31], P. Vannerem[10], R. Vértesi[30,e], M. Verzocchi[17], H. Voss[8,q], J. Vossebeld[8,h], C.P. Ward[5], D.R. Ward[5], P.M. Watkins[1], A.T. Watson[1], N.K. Watson[1], P.S. Wells[8], T. Wengler[8], N. Wermes[3], G.W. Wilson[16,k], J.A. Wilson[1], G. Wolf[24], T.R. Wyatt[16], S. Yamashita[23], D. Zer-Zion[4], L. Zivkovic[24]

[1]School of Physics and Astronomy, University of Birmingham, Birmingham B15 2TT, UK
[2]Dipartimento di Fisica dell' Università di Bologna and INFN, I-40126 Bologna, Italy
[3]Physikalisches Institut, Universität Bonn, D-53115 Bonn, Germany
[4]Department of Physics, University of California, Riverside CA 92521, USA
[5]Cavendish Laboratory, Cambridge CB3 0HE, UK
[6]Ottawa-Carleton Institute for Physics, Department of Physics, Carleton University, Ottawa, Ontario K1S 5B6, Canada
[8]CERN, European Organisation for Nuclear Research, CH-1211 Geneva 23, Switzerland
[9]Enrico Fermi Institute and Department of Physics, University of Chicago, Chicago IL 60637, USA
[10]Fakultät für Physik, Albert-Ludwigs-Universität Freiburg, D-79104 Freiburg, Germany
[11]Physikalisches Institut, Universität Heidelberg, D-69120 Heidelberg, Germany
[12]Indiana University, Department of Physics, Bloomington IN 47405, USA
[13]Queen Mary and Westfield College, University of London, London E1 4NS, UK

[14]Technische Hochschule Aachen, III Physikalisches Institut, Sommerfeldstrasse 26-28, D-52056 Aachen, Germany
[15]University College London, London WC1E 6BT, UK
[16]Department of Physics, Schuster Laboratory, The University, Manchester M13 9PL, UK
[17]Department of Physics, University of Maryland, College Park, MD 20742, USA
[18]Laboratoire de Physique Nucléaire, Université de Montréal, Montréal, Québec H3C 3J7, Canada
[19]University of Oregon, Department of Physics, Eugene OR 97403, USA
[20]CCLRC Rutherford Appleton Laboratory, Chilton, Didcot, Oxfordshire OX11 0QX, UK
[21]Department of Physics, Technion-Israel Institute of Technology, Haifa 32000, Israel
[22]Department of Physics and Astronomy, Tel Aviv University, Tel Aviv 69978, Israel
[23]International Centre for Elementary Particle Physics and Department of Physics, University of Tokyo, Tokyo 113-0033, and Kobe University, Kobe 657-8501, Japan
[24]Particle Physics Department, Weizmann Institute of Science, Rehovot 76100, Israel
[25]Universität Hamburg/DESY, Institut für Experimentalphysik, Notkestrasse 85, D-22607 Hamburg, Germany
[26]University of Victoria, Department of Physics, P O Box 3055, Victoria BC V8W 3P6, Canada
[27]University of British Columbia, Department of Physics, Vancouver BC V6T 1Z1, Canada
[28]University of Alberta, Department of Physics, Edmonton AB T6G 2J1, Canada
[29]Research Institute for Particle and Nuclear Physics, H-1525 Budapest, P O Box 49, Hungary
[30]Institute of Nuclear Research, H-4001 Debrecen, P O Box 51, Hungary
[31]Ludwig-Maximilians-Universität München, Sektion Physik, Am Coulombwall 1, D-85748 Garching, Germany
[32]Max-Planck-Institute für Physik, Föhringer Ring 6, D-80805 München, Germany
[33]Yale University, Department of Physics, New Haven, CT 06520, USA

[a] and at TRIUMF, Vancouver, Canada V6T 2A3
[b] now at University of Iowa, Dept of Physics and Astronomy, Iowa, U.S.A.
[c] and Institute of Nuclear Research, Debrecen, Hungary
[d] now at Institute of Physics, Academy of Sciences of the Czech Republic, 18221 Prague, Czech Republic
[e] and Department of Experimental Physics, University of Debrecen, Hungary
[f] and MPI München
[g] and Research Institute for Particle and Nuclear Physics, Budapest, Hungary
[h] now at University of Liverpool, Dept of Physics, Liverpool L69 3BX, U.K.
[i] now at Dept. Physics, University of Illinois at Urbana-Champaign, U.S.A.
[j] and Manchester University Manchester, M13 9PL, United Kingdom
[k] now at University of Kansas, Dept of Physics and Astronomy, Lawrence, KS 66045, U.S.A.
[l] now at University of Toronto, Dept of Physics, Toronto, Canada
[m] current address Bergische Universität, Wuppertal, Germany
[n] now at University of Mining and Metallurgy, Cracow, Poland
[o] now at University of California, San Diego, U.S.A.
[p] now at The University of Melbourne, Victoria, Australia
[q] now at IPHE Université de Lausanne, CH-1015 Lausanne, Switzerland
[r] now at IEKP Universität Karlsruhe, Germany
[s] now at University of Antwerpen, Physics Department,B-2610 Antwerpen, Belgium; supported by Interuniversity Attraction Poles Programme – Belgian Science Policy
[u] and High Energy Accelerator Research Organisation (KEK), Tsukuba, Ibaraki, Japan
[v] now at University of Pennsylvania, Philadelphia, Pennsylvania, USA
[w] now at TRIUMF, Vancouver, Canada
[x] now at DESY Zeuthen

[y] now at CERN
[z] now at DESY
[*] Deceased

1 Introduction

Hadronic data in e^+e^- collisions can be characterised by event shape distributions and inclusive observables such as charged particle multiplicities and momentum spectra. Measurement of the detailed properties of the hadronic sector of W^+W^- decays allows the question of "colour reconnection" (CR) [1] to be addressed experimentally, in addition to providing tests of Monte Carlo models. The decay products of the two W boson decays have a significant space-time overlap as the separation of their decay vertices at LEP2 energies is small compared to characteristic hadronisation distance scales. In the fully hadronic channel this may lead to new types of final state interactions. Colour reconnection is the general name applied to the case where such final state interactions lead to colour exchange between the decay products of the two W bosons. A modification of the colour flow in this way could have a significant influence on the measured mass of the W boson, as first noted in [1]. It is therefore essential to ascertain whether or not such effects are present in W decays. As described in [2], a precedent is set for such effects in colour suppressed B meson decays, *e.g.* $B \to J/\psi K$, where there is "cross-talk" between the two original colour singlets, $\bar{c}$+s and c+spectator.

There is general consensus that observable effects of such interactions during the perturbative phase are expected to be small [2]. In contrast, significant interference in the hadronisation process is considered to be a real possibility. With the current understanding of non-perturbative QCD, such interference can be estimated only in the context of specific models [1–10]. Other final state effects such as Bose-Einstein correlations (BEC) between identical bosons from different W decays may also influence the observed event properties.

This paper presents two different measurements which are sensitive to colour reconnection effects. The inclusive properties of W^+W^- decay products have been measured [11–13] and found to have limited sensitivity to colour reconnection using the data available at LEP2. Characteristic observables such as the inclusive charged particle multiplicity in $W^+W^- \to q\overline{q}q\overline{q}$ events, $\langle n_{\mathrm{ch}}^{4q} \rangle$, and its centre-of-mass energy dependence have been widely used to quantify the effect of colour reconnection in W^+W^- events [1–6, 8–10], and are therefore studied in this paper. As in [12], the hadronic part of $W^+W^- \to q\overline{q}\ell\overline{\nu}_\ell$ events is compared with $W^+W^- \to q\overline{q}q\overline{q}$ events, while the leptonically decaying W is excluded.

More recently, all LEP collaborations have concentrated on studies of "particle flow" [14–16], a generalisation of the well-known "string effect" [17] to the four-jet case of $W^+W^- \to q\overline{q}q\overline{q}$, as models predict [18] this has a larger sensitivity to colour reconnection. This analysis compares the density of charged particles in two regions: the first, between pairs of hadronic jets originating from the same W boson, and the second, between pairs of hadronic jets which originate from different W bosons. In the absence of colour exchange between the two W bosons, the particle density is expected to be larger in the first region. Colour reconnection would lead to a migration of particles into the second region, in addition to a change in the total multiplicity. All data in the range 189–209 GeV are studied using the particle flow method in this paper, which supersedes previous OPAL analyses on the subject [11, 12].

This paper is organised as follows: Section 2 summarises data and Monte Carlo models used, Section 3 describes the inclusive charged particle and particle flow analyses and Section 4 the estimation of systematic effects. Sections 5 and 6 discuss the results and draw conclusions.

2 Data Selection and Monte Carlo Models

This paper uses data corresponding to an integrated luminosity of approximately 625 pb^{-1} recorded during 1998–2000 with the OPAL detector, which is described fully elsewhere [19]. The data are separated into samples at six centre-of-mass energies, varying between approximately 189 GeV and 209 GeV. Those accumulated above 202.5 GeV are considered at a single luminosity weighted mean centre-of-mass energy of 206.0 GeV. The selection criteria and distribution of data by $\mathrm{W^+W^-}$ final state, luminosity and centre-of-mass energy are given in [20], with a total of 5401 $\mathrm{W^+W^-} \to \mathrm{q\overline{q}q\overline{q}}$ and 2757 $\mathrm{W^+W^-} \to \mathrm{q\overline{q}}\ell\overline{\nu}_\ell$ candidates selected. Only $\mathrm{W^+W^-} \to \mathrm{q\overline{q}}\ell\overline{\nu}_\ell$ events in which the charged lepton was identified as an electron or a muon are used, to ensure that the charged particle multiplicity of the hadronically decaying W is well understood.

It is essential to have reliable selection of charged particles in the detector in this analysis. Charged particles may have up to 159 hits in the principal tracking chamber, the jet chamber. Tracks used in the analysis are required to have a minimum of 40 hits in the $|\cos\theta|$ region[1] in which at least 80 are possible. At larger $|\cos\theta|$, the number of hits is required to be at least 50% of the expected number and not fewer than 20, corresponding to a fiducial acceptance of $|\cos\theta| < 0.96$. Tracks must have a momentum component in the plane perpendicular to the beam axis of greater than 0.15 GeV/c, and a measured momentum p of less than 100 GeV/c. For each track, the point of closest approach to the collision axis is found, and the distance between this point and the average interaction point is required to be less than 2 cm in the r-ϕ plane and less than 25 cm in z. Clusters of energy in the electromagnetic calorimeter are required to have a measured energy greater than 0.10 GeV if they occur in the barrel region of the detector ($|\cos\theta| < 0.82$), and greater than 0.25 GeV if they occur in the endcaps ($0.82 < |\cos\theta| < 0.98$).

Most samples of Monte Carlo events used in this paper include detailed simulation of the OPAL detector [21] and of initial state photon radiation and have been passed through the same selection and analysis procedures applied to the data ("detector level"). A second class of samples does not include initial state photon radiation or simulation of the detector and allows all particles with lifetimes shorter than 3×10^{-10} s to decay ("hadron level").

Detector level samples were generated for a default set of physics processes at all centre-of-mass energies considered. Additional samples were generated for systematic studies as described in Section 2.4. Hadron level samples were produced for all variants of $\mathrm{W^+W^-}$ events[2] considered (different hadronisation and colour reconnection models) at all centre-of-mass energies. The Monte Carlo event generators used to simulate the physics processes are described in the remainder of this Section, with emphasis on the CR models themselves.

The effects of colour reconnection are implemented in several $\mathrm{W^+W^-}$ event generators, and three groups of such models are studied, namely those of Sjöstrand and Khoze (SK) [2, 22], and those implemented in ARIADNE 4.11 [5,6] and in HERWIG 6.2 [7,8]. Events from all CR models used in this paper have been generated in conjunction with the electroweak generator KORALW 1.42 (KW) [23]. For the SK models, samples of events were generated such that they are identical to the conventional KORALW $\mathrm{W^+W^-} \to \mathrm{q\overline{q}q\overline{q}}$ events up to the end of the parton shower. This allows the construction of samples with an arbitrary fraction of reconnected events (including detector simulation) for the SK-I model, and also improves the statistical precision of studies using the SK models, such as estimation

[1] The OPAL coordinate system is defined such that the origin is at the geometric centre of the jet chamber, z is parallel to, and has positive sense along, the $\mathrm{e^-}$ beam direction, r is the coordinate normal to z, θ is the polar angle with respect to $+z$ and ϕ is the azimuthal angle around z.

[2] In this paper, "$\mathrm{W^+W^-}$ events" implies doubly-resonant W pair production diagrams, *i.e.* t-channel ν_e exchange and s-channel Z^0/γ exchange, referred to as "CC03" in [14].

of CR bias in measurements of the W boson mass [20]. For other CR models, the electroweak process was generated using KORALW and then a single set of events was hadronised by each of HERWIG and the ARIADNE models. The same KORALW events were also hadronised using the conventional QCD models of Section 2.4. All models considered have been tuned to describe Z^0 data, as described in [20].

2.1 SK CR Models

The SK models are based upon the Lund string picture of colour confinement, in which a string is created that spans the decay product partons associated with each W. These strings expand from the respective decay vertices and subsequently fragment to hadrons. Before this occurs, at most one reconnection is allowed between sections of the two strings. The main scenarios considered are called type I (SK-I) and type II (SK-II) in analogy to the two types of superconducting vortices which could correspond to colour strings. In the SK-I scenario, the two colour flux tubes have a lateral extent comparable to hadronic dimensions. The probability for reconnection to occur is given by $P^{\rm reco} = (1 - \exp(-Vk_I))$, where V is the space-time integrated product of the maximum colour field strengths of the two overlapped W strings and k_I is a free (dimensionless) strength parameter. In the SK-II scenario, the strings have infinitesimally small radii and a unit reconnection probability upon their first crossing. A third scenario considered, SK-II$'$, is similar to SK-II but reconnection is only allowed to occur at the first string crossing which would reduce the total string length of the system.

As described in [22], the only tuning necessary for these models is to ensure that the JETSET hadronisation model gives a good description of Z^0 data: parameters governing the behaviour of the reconnection model are not adjusted to fit data. Therefore, the same parameters were used as for the corresponding sample of non-reconnected $e^+e^- \to W^+W^-$ events. The parton shower cut-off parameter, Q_0, to which the predictions of the SK-II and SK-II$'$ models in particular are sensitive, is set to 1.9 GeV in the OPAL tune [24] of the JETSET hadronisation model. The fractions of $W^+W^- \to q\bar{q}q\bar{q}$ events in which reconnection occurs at $\sqrt{s} = 199.5$ GeV, $P^{\rm reco}$, are predicted to be 17.2% for SK-II and 16.1% for SK-II$'$. As the fraction of events reconnected varies with k_I in the SK-I model, two illustrative values of k_I are given for comparison in figures and tables: $k_I = 0.9$, giving a fraction of reconnected events, $P^{\rm reco} \simeq 34.3\%$, comparable to that used in [2], and an extreme case of $k_I = 100$ ($P^{\rm reco} \simeq 98\%$). The latter will be referred to hereafter as SK-I with 100% CR.

Samples of these three models including simulation of the detector were generated at $\sqrt{s} =$ 188.6 GeV, 199.5 GeV and 206.0 GeV.

2.2 ARIADNE CR Models

The second set of CR models is contained in the ARIADNE Monte Carlo program. They may be considered as extensions of the earlier partonic dipole model[3] [4], as both models were implemented using the ARIADNE Monte Carlo program and the same criterion is employed in the reconnection ansatz to determine whether reconnection is allowed. Perturbative QCD favours configurations with minimal string length in hadronic Z^0 decays [14]. When the partons of two W bosons are separating and strings are being formed between them, it is plausible that configurations corresponding to a reduced total string length are favoured. In the reconnection model of ARIADNE, the string length is defined in terms of the Λ measure, which may be viewed as the rapidity range along the string:

[3] In [4], at most one reconnection was allowed per event and possible reconnections between the decay products of a single W were not implemented.

$\Lambda = \sum_i \ln(m_i^2/m_\rho^2)$, where m_i is the invariant mass of string segment i and m_ρ sets a typical hadronic mass scale. Reconnections are only permitted if they satisfy the constraints of colour algebra and also lead to a reduction in the total Λ of the system. The first model is a variant of ARIADNE in which rearrangement of the colour flow is allowed but is restricted to the decay products of each W separately. This is referred to as AR-1. The second ARIADNE model, referred to herein as AR-2, is the same as AR-1 but in addition allows reconnections between the two W bosons for gluons having energies, $E_g < \Gamma_W$, while the third ARIADNE model, AR-3, does not impose such a restriction. As gluons emitted with $E_g > \Gamma_W \sim 2$ GeV are perturbative in nature and have been shown to be radiated incoherently by the two initial colour dipoles [2], the model AR-3 is disfavoured on theoretical grounds. In addition, the ARIADNE colour reconnection models have been shown to be disfavoured by $Z^0/\gamma \to q\overline{q}$ data [25]. The AR-3 model is therefore not considered further in this paper.

The way in which CR is implemented in AR-2 leads to an artificial difference relative to the AR-1 model which is not directly related to reconnections between the two W systems. In AR-2, the dipole cascade (ordering in transverse momentum) is run in two stages from the maximum allowed gluon energy down to the cutoff: once down to $E_g = \Gamma_W$ allowing only reconnections within a single W system, and then a second time allowing $E_g < \Gamma_W$ and cross-talk between the two W systems. In AR-1, the dipole cascade is carried out in a single stage without any interruption down to the cutoff. As noted in [5], the AR-2 scheme is not strictly consistent with the assumptions of ordering in transverse momentum in the dipole cascade model and this leads to the observable differences between AR-2 and AR-1 referred to above. To ensure that differences between these two models are only due to inter-W reconnections, the dipole cascade in AR-1 is modified to run in two stages with an interruption at $E_g = \Gamma_W$ [26].

As the same tuning of model parameters is used for both AR-1 and AR-2, and no colour flow takes place between the two W bosons in events in the AR-1 model, the AR-1 model serves as the no-CR model when estimating the expected sensitivity of the measurements to colour reconnection. The AR-1 model is also used as an alternative model when estimating systematic effects in the hadronisation of the W decay products.

Samples of the AR-1 and AR-2 models including simulation of the detector were generated at $\sqrt{s} = 199.5$ GeV, with the fraction of $W^+W^- \to q\overline{q}q\overline{q}$ events in which reconnection occurs being approximately 49.4% for AR-2.

2.3 HERWIG CR Model

The third model is contained in the HERWIG program and provides an alternative CR model based on cluster hadronisation. In the cluster model, quarks and gluons from the perturbative parton shower evolution are combined locally into colour singlet objects called clusters which have (relative to strings) low mass and small space-time extent, each cluster decaying directly into a small number of hadrons. In the CR version of this model, an alternative pattern of cluster formation is implemented after the parton shower and gluon splitting phase. In this, new associations of partons into clusters are considered where they would lead to a smaller space-time extent of the clusters. When such viable alternative parton-cluster associations exist, they occur with a probability equal to $\frac{1}{9}$ $(= 1/N^2_{\text{colours}})$. A sample of events including simulation of the detector was generated at $\sqrt{s} = 199.5$ GeV, with reconnection occurring in approximately 23% of $W^+W^- \to q\overline{q}q\overline{q}$ events.

2.4 No-CR Monte Carlo Samples

The models used are the same as those in [20], where a more detailed description can be found, and all are generated at the detector level. Samples of W^+W^- events without colour reconnection effects are simulated at all centre-of-mass energies using the KORALW Monte Carlo, with fragmentation carried out using the JETSET 7.408 model. At three centre-of-mass energies (188.6 GeV, 199.5 GeV, 206.0 GeV), additional samples are used in which the underlying W^+W^- production process is simulated by KORALW, while the fragmentation of a given set of four fermions is performed by either HERWIG, ARIADNE or an older parameter set of JETSET derived from tuning the model to OPAL inclusive event shape data, as used in [27]. Hereafter, these samples are referred to as JETSET, HERWIG, ARIADNE and "old JETSET", respectively. Samples of W^+W^- events including Bose-Einstein correlations are simulated using the LUBOEI model [28] in PYTHIA 6.125 [3].

The dominant backgrounds in the $W^+W^- \to q\overline{q}q\overline{q}$ channel are $e^+e^- \to Z^0/\gamma \to q\overline{q}$ with radiation of energetic gluons, and four-fermion final states, primarily $e^+e^- \to (Z^0/\gamma)(Z^0/\gamma) \to q\overline{q}q\overline{q}$. Backgrounds in the $W^+W^- \to q\overline{q}\ell\overline{\nu}_\ell$ channel are significantly lower from all sources and receive small additional contributions from $e^+e^- \to Z^0/\gamma \to \tau^+\tau^-$, simulated using the KK2f version 4 Monte Carlo program [29]. For completeness, the small background represented by hadronic two-photon events is simulated using the PHOJET [30] and HERWIG event generators.

Four samples of two-fermion processes $e^+e^- \to Z^0/\gamma \to q\overline{q}$ are simulated at each centre-of-mass energy, to allow systematic uncertainties to be estimated: in three samples the hard process is generated using KK2f, with fragmentation of the quarks performed by each of JETSET, HERWIG and ARIADNE, while in a fourth sample both the hard process and fragmentation are generated by PYTHIA 6.125.

Four-fermion processes are modelled using the KORALW 1.42 Monte Carlo, which contains matrix elements calculated by grc4f 2.0 [31]. The complete four-fermion samples are divided into two categories: "WW-like four-fermion events", corresponding to final states which could have been produced by diagrams involving at least one W boson, and "ZZ events", which are the complementary sample, not all of which involve two Z bosons.

In this and similar analyses, $(Z^0/\gamma)(Z^0/\gamma) \to q\overline{q}q\overline{q}$ events are considered as background. In general, the susceptibility to the effects of CR in such events is expected to be comparable to that in $W^+W^- \to q\overline{q}q\overline{q}$. A more complete treatment of such events would require implementation of the CR models in a full four-fermion generator, thereby obviating the need explicitly to subtract ZZ four quark final states. Although this is not done, it is expected to have only a small effect as the background level from $(Z^0/\gamma)(Z^0/\gamma) \to q\overline{q}q\overline{q}$ events is low (less than 5% in the particle flow analysis).

This four-fermion "background" is constructed from the difference between the predictions of two classes of events generated using the KORALW model: one containing the full set of interfering four-fermion diagrams (WW-like four-fermion events and ZZ events), the other containing only the W pair production diagrams.

Alternative modelling of the four-fermion process with a more complete treatment of so-called $O(\alpha)$ photon radiation has been studied using samples generated by the KandY generator [32] which incorporates KORALW 1.51 [32] and YFSWW3 [33].

3 Data Analysis and Correction Procedure

The measurements of the inclusive charged particle multiplicity and of the particle flow are described below. The former is a fully inclusive measurement and data are corrected for the effects of finite detector resolution and acceptance, whereas the latter compares the predictions of a variety of models with the data at detector level.

3.1 Inclusive Charged Particle Multiplicity

The analysis of charged particle multiplicity follows the unfolding procedure described in [12]. The distributions of particle multiplicity and of the scaled charged particle momentum, $x_p = p/E_{\rm beam}$, where $E_{\rm beam}$ is the beam energy, are used to measure the mean charged particle multiplicities in $\mathrm{W^+W^-} \to \mathrm{q\overline{q}q\overline{q}}$ events ($\langle n_{\rm ch}^{\rm 4q}\rangle$) events, and in $\mathrm{W^+W^-} \to \mathrm{q\overline{q}}\ell\overline{\nu}_\ell$ events ($\langle n_{\rm ch}^{\rm qq\ell\nu}\rangle$), and their difference ($\Delta\langle n_{\rm ch}\rangle = \langle n_{\rm ch}^{\rm 4q}\rangle - 2\langle n_{\rm ch}^{\rm qq\ell\nu}\rangle$).

Figures 1 and 2 show the uncorrected multiplicity and x_p distributions for $\mathrm{W^+W^-}$ candidate events before background subtraction. The background predictions are the sum of all other Standard Model processes, as described by the models outlined in Section 2.4. The data are described reasonably well by all $\mathrm{W^+W^-}$ models including conventional QCD processes alone, and by those including CR. Integration of the x_p distribution is used for the principal measurement of mean charged particle multiplicity as it has slightly lower estimated systematic effects than the direct multiplicity measurement, which is therefore used as a cross-check.

The x_p distribution is corrected for contamination using a bin-by-bin subtraction of the expected background, based on Monte Carlo estimates. Corrections are then applied for finite acceptance and the effects of detector resolution, using two samples of $\mathrm{e^+e^-} \to \mathrm{W^+W^-}$ events generated using the same Monte Carlo event generator at the same $\sqrt{s}$, one at hadron level, the other at detector level. Distributions normalised to the number of events at the detector and the hadron level are compared to derive bin-by-bin correction factors which are used to correct the observed x_p distribution at each centre-of-mass energy.

This bin-by-bin unfolding procedure is suitable for x_p as the effects of finite resolution and acceptance do not cause significant migration (and therefore correlation) between bins. Such a method is not readily applicable to multiplicity distributions, due to the large correlations between bins. Instead, a matrix correction is used to correct for detector resolution effects, followed by a bin-by-bin correction which accounts for the residual effects due to acceptance cuts and initial state radiation, as in previous OPAL multiplicity studies, e.g. [12, 34].

Figure 3 shows the corrected values of mean charged particle multiplicity, $\langle n_{\rm ch}^{\rm 4q}\rangle$, $\langle n_{\rm ch}^{\rm qq\ell\nu}\rangle$ and their difference $\Delta\langle n_{\rm ch}\rangle$ as a function of centre-of-mass energy. It can be seen that, although the no-CR models vary in their predictions for both $\langle n_{\rm ch}^{\rm 4q}\rangle$ and $\langle n_{\rm ch}^{\rm qq\ell\nu}\rangle$, they are in complete agreement that the value of $\Delta\langle n_{\rm ch}\rangle$ is negligibly small, in contrast to the CR models shown in Figure 3(c). However, the predictions of both conventional QCD models and models of CR are found to be compatible with the data within uncertainties. As the multiplicity data are not observed to vary significantly with $\sqrt{s}$, measurements from all centre-of-mass energies are combined assuming they are independent of $\sqrt{s}$. The combined results are presented in Table 1, systematic uncertainties discussed in Section 4, and quantitative comparisons with models presented in Table 2.

3.2 Particle Flow

The analysis of event properties presented here is a generalisation of the string effect analysis in three-jet $e^+e^- \to q\overline{q}g$ events to the four-jet topology of $W^+W^- \to q\overline{q}q\overline{q}$. The situation is necessarily more complicated in the $W^+W^- \to q\overline{q}q\overline{q}$ channel because, in contrast to the three-jet case, events are not constrained by momentum conservation to be planar. The analysis is therefore carried out in four distinct planes, each of which is defined by a pair of jet axes. Charged particles and clusters of electromagnetic energy, selected as in [12], are combined into four jets using the $k_\perp$ [35] jet-finding algorithm, and the total momentum and energy of each of the jets are corrected empirically for double counting using the same energy flow algorithm employed in [20]. The jet momenta are further modified by a kinematic fit, imposing the four constraints of energy and momentum conservation, to obtain an improved estimate of the trajectories of the underlying four fermions from the W^+W^- decays. To ensure that a relatively simple colour topology is being studied, events having a five-jet like topology[4] are rejected. This is also expected to lead to a better description of the dominant $e^+e^- \to q\overline{q}$ background events by the parton shower models.

The analysis proceeds in three stages, namely: association of pairs of jets with W bosons and definition of four planes, projection of charged particles onto these planes, and comparison of the distributions of particles in these planes. Each of these aspects of the analysis is described below.

The association between pairs of jets and W bosons is performed using a minor variant of the algorithm that was introduced in [27]. In the current scheme, the mass obtained from a five-constraint[5] kinematic fit [20] is combined with the variables of [27] into a single likelihood discriminant, selecting the correct pairing of jets to W bosons with a purity of $\sim 90\%$. The total number of events used in the analysis after all selections is 2199, with an overall efficiency for selecting $W^+W^- \to q\overline{q}q\overline{q}$ of $\sim 40\%$. Small variations in performance with centre-of-mass energy are detailed in Table 3.

The pairing of jets originating from the same parent W defines two intra-W planes, as illustrated in Figure 4. With four jets, there exist two ways in which planes may be defined between jets which originate from different W boson (inter-W regions). The configuration which results in the smaller sum of inter-W angles is chosen. The motivation for this is the suggestion [2, 4, 5] that colour reconnection is more probable for topologies in which jets from different W bosons are close together in angle. In such a configuration, a rearrangement of the colour flow in the event would be energetically favoured due to a reduction in the overall "length" of the colour flux tubes.

Reconstructed charged particles in the event are projected onto the intra-W and inter-W planes as follows, and illustrated in Figure 4. The first plane examined is that defined by the most energetic jet in the event ('jet 1') and the jet belonging to the same W ('jet 2'), as given by the jet pairing algorithm. The next plane considered is that between jet 2 and a jet ('jet 3') from the other W, such that the sum of inter-W angles is minimal. The third plane is the other intra-W region between jet 3 and the remaining jet in the event, 'jet 4'. The final plane is that between jet 4 and jet 1.

All charged particles in an event are projected onto each of the four planes in turn. In each plane, an azimuthal angle $0 < \chi_1 < 2\pi$ is defined, having positive sense between pairs of jets as described above and indicated in Figure 4. To account for the variation in the angle between pairs of jets, the distribution of particles is evaluated as a function of χ_1 for each plane after rescaling, event-by-event, to the angle between the jets which define the plane, χ_0. This gives a normalised angle, $\chi_R = \chi_1/\chi_0$, where $\chi_R \equiv 0$ corresponds to the jet axis of the lower number jet which defines the plane. Particles

[4] Following [20], five-jet events are classified as those in which the $k_\perp$ jet resolution parameter for the four-jet to five-jet transition, y_{45}, satisfies $\log(y_{45}) > -5.6$.

[5] The additional constraint imposed is equality of the masses of the two W boson candidates.

outside the inter-jet region, *i.e.*, having $\chi_R > 1$, are not considered further. In the case where a particle is projected into the inter-jet region of more than one plane, it is exclusively assigned to the plane relative to which it has the smallest transverse momentum.

The four normalised inter-jet regions are combined in a single distribution in the range $0 < \chi < 4$, as shown in Figure 5(a), where the structure of the four jets is apparent. The variable χ is defined as $\chi = \chi_R + (n_{\rm plane} - 1)$, where $n_{\rm plane}$ is an integer between 1 and 4, corresponding to the four planes in the order given, and as shown in Figure 4.

As seen in Figure 5(a), the data are consistent with the predictions of $\mathrm{W^+W^-}$ production using the conventional hadronisation models plus the sum of all background processes. Figure 5(b) compares the sum of background-subtracted data with predictions from various CR models. The data are found to be adequately described by models, with the exception of the extreme scenario of the SK-I model, which predicts lower particle densities in the intra-W regions, and higher particle densities in the inter-W regions.

In conventional QCD models without interaction of the colour fields between the $\mathrm{W^+}$ and $\mathrm{W^-}$, the particle density (or particle flow) is expected to be higher in the intra-W regions, $0 < \chi < 1$ and $2 < \chi < 3$ than in the inter-W regions. After a rearrangement, in addition to a change in absolute number of charged particles in the event, there may be a migration of particle flow away from these regions in favour of the inter-W regions, $1 < \chi < 2$ and $3 < \chi < 4$. Consequently, one way of studying the effects of colour rearrangement is to compare the particle flow of the two intra-W regions to that of the two inter-W regions. As the properties of the two inter-W regions should both be affected by colour rearrangement in the same way, these are added together, as are the two intra-W regions. The ratio of intra-W to inter-W particle flow distributions is then formed,

$$R_{\rm flow} = \frac{\frac{{\rm d}n_{\rm ch}}{{\rm d}\chi_R}({\rm intra-W})}{\frac{{\rm d}n_{\rm ch}}{{\rm d}\chi_R}({\rm inter-W})},$$

where $n_{\rm ch}$ is the number of charged particle tracks projected into a given inter-jet region.

Figure 6(a) compares the measured values of this ratio using all data (after background subtraction) with the predictions of conventional hadronisation models, while Figure 6(b) shows data compared with the predictions of various CR models.

Differences between the data and models, and consistency between the predictions of different models, are more apparent in Figure 6 than in Figure 5. The data are found to lie slightly below the model predictions in the region away from the jet cores for conventional QCD Monte Carlo models and most CR models. While the SK-I model with $k_I = 100$ shows significant separation from data and the other models, it is apparent that the predicted effects of CR in the other SK models are limited.

3.2.1 Quantitative Measures of CR

To quantify the consistency between data and predictions of models, the ratio of the integral of the particle flow in the intra-W regions to the integral of particle flow in the inter-W regions,

$$R_N = \frac{\int_{0.2}^{0.8} \frac{{\rm d}n_{\rm ch}}{{\rm d}\chi_R}({\rm intra-W}){\rm d}\chi_R}{\int_{0.2}^{0.8} \frac{{\rm d}n_{\rm ch}}{{\rm d}\chi_R}({\rm inter-W}){\rm d}\chi_R} \qquad (1)$$

is formed. This is a traditional observable used in string effect studies, *e.g.* [17], and is sensitive to differences in the number of particles in the inter-jet regions but relatively insensitive to their angular distribution and the choice of binning.

The limits of integration are chosen to optimise the predicted sensitivity in the SK-I model at $\sqrt{s}$=189 GeV. This choice also allows the uncertainty on the ratio to be calculated from error propagation. In the case where the limits are extended too close to the cores of the jets, a significant correlation is introduced between neighbouring inter-jet regions and the error calculation is no longer valid. It is to be noted that to calculate the uncertainty correctly, the numerator and denominator of Equation 1 must be evaluated event-by-event, rather than by integration of distributions such as Figure 5. The validity of the statistical errors has been tested using data-sized samples from a variety of Monte Carlo models, each with more than 90 times the statistics of the entire 189–209 GeV data sample.

To estimate the sensitivity to colour reconnection effects, the R_N predicted by each colour reconnection model is compared with that obtained from the corresponding "no reconnection" scenario of the same model. As a guide to the performance of the analysis, the predicted statistical sensitivity of the analysis is summarised in Table 4 using model predictions at $\sqrt{s}$ = 199.5 GeV. The fraction of reconnected events in each model is also shown. The sensitivity is defined as the difference between a given reconnection model and its corresponding "no reconnection" sample (ΔR_N), divided by the expected statistical uncertainty obtained using all data presented in this paper ($\sigma^{\mathrm{stat.}}_{R_N}$). It can be seen that there is a significant sensitivity to the extreme scenario of the SK-I model in which almost all events are reconnected but limited sensitivity to all other CR models considered.

To combine the observed R_N from different centre-of-mass energies, an assumption has to be made about possible energy dependence of the measurements. Figure 7 shows the measured values of R_N together with the predictions of the JETSET and other Monte Carlo samples. Although some models exhibit an energy dependent R_N, the variations are small compared to the statistical uncertainties in data. Measurements are therefore combined assuming they are independent of $\sqrt{s}$, and the impact of this is considered as a systematic effect. Quantitative comparisons of the combined R_N in data are made using predictions of all models studied at $\sqrt{s}$ = 199.5 GeV, at which energy a complete set of Monte Carlo samples is available. On the scale of variations predicted in R_N, this $\sqrt{s}$ is close to the luminosity-weighted centre-of-mass energy of 197.8 GeV.

4 Systematic Uncertainties

Systematic uncertainties are studied using measurements averaged over $\sqrt{s}$, and are shown in Tables 1 and 5 for the inclusive charged particle multiplicity and particle flow analyses, respectively. Sources of systematic error considered include hadronisation effects in the $\mathrm{W^+W^-}$ models, detector effects related to tracking of charged particles and background subtraction. The analysis of mean particle multiplicities involves the unfolding of observed data to the hadron level and a possible additional uncertainty related to this procedure is studied. The particle flow analysis is performed using ratios of sums and no unfolding of the data is performed, and so many systematic effects are expected to cancel or be negligibly small.

4.1 $\mathrm{W^+W^-}$ Hadronisation

For the multiplicity analysis, samples of simulated $\mathrm{W^+W^-}$ events incorporating JETSET hadronisation are treated as background-subtracted data and unfolded with each of the alternative $\mathrm{W^+W^-}$ hadronisation models and colour reconnection models. The CR models are included in this procedure to allow for the possibility that such effects are present in the underlying physics. Where samples of

a given model exist at more than one $\sqrt{s}$ the results of unfolding are averaged. The uncertainty is assigned as the largest difference between the values obtained when unfolding JETSET events with the default model (JETSET) and with any of the alternative models, and is dominated by the HERWIG models.

For the particle flow analysis, this error is assigned by using samples of W^+W^- events generated using KORALW, and hadronised with each of the models JETSET, HERWIG, ARIADNE, old JETSET and AR-1. Where samples of a given model exist at more than one $\sqrt{s}$ the results are averaged. Each model is treated as background-subtracted data, and the uncertainty is assigned as half of the maximum difference between the R_N predicted by any pair of models. This differs from the definition used for the multiplicity analysis: as no unfolding is performed, there is no default model against which to study systematic effects. It can be seen from Figure 7 that this uncertainty is determined by differences between the HERWIG and old JETSET hadronisation models.

4.2 BEC

While the presence of Bose-Einstein correlations among particles originating from the same hadronically decaying W boson (intra-W BEC) has been unambiguously established [36], there is no significant evidence for BEC between particles originating from different W bosons (inter-W BEC) [37,38]. However, these are not excluded and, following [38] and [20], a systematic error corresponding to 77% of the effect of (inter-W BEC) − (intra-W BEC) on the measurement is assigned. In the multiplicity analysis, the uncertainty was assigned as 77% of the difference in the hadron level multiplicity obtained when the inter-W BEC and intra-W BEC samples were each treated as background-subtracted data. In the particle flow analysis the uncertainty was assigned as 77% of the difference between the R_N values predicted by the inter-W BEC model and the intra-W BEC model.

4.3 Track Definition

Uncertainties arising from the selection of charged tracks are estimated by examining the stability of the difference between data and Monte Carlo predictions for multiplicity or R_N. Both analyses are repeated three times, with track selection criteria varied within reasonable limits [12]. The maximum allowed values of the distances of closest approach to the interaction region in r-ϕ and z are varied from 2 cm to 5 cm and from 25 cm to 50 cm, respectively, and the minimum number of hits on tracks is varied from 20 to 40. The uncertainty on the charged track definition is the sum in quadrature of these three effects. This source represents a significant systematic effect and is dominated by the variation of the minimum number of hits required to form a track.

4.4 Background

Alternative models and cross-sections were used to estimate uncertainties associated with the background subtraction. The uncertainty is formed using the difference between the measured multiplicities (or R_N values) obtained using the alternative background models and that obtained using the default background model and assumed cross-section at each centre-of-mass energy.

4.4.1 $e^+e^- \to q\overline{q}$ Modelling

Uncertainties in generation of the hard process and hadronisation may affect the shape of the background and are estimated by comparing models. A sample of $e^+e^- \to q\overline{q}$ events, generated using KK2f and hadronised with each of JETSET, HERWIG and ARIADNE, is available at all centre-of-mass energies studied, as is a sample generated entirely using PYTHIA. This uncertainty is assigned as the largest difference between the result obtained using any model and the result obtained when the default JETSET model is used.

4.4.2 $e^+e^- \to q\overline{q}$ Rate

This uncertainty arises due to imperfect knowledge of the accepted background cross-section. It is evaluated using the deviations in the measurements caused when the $e^+e^- \to q\overline{q}$ background rate is varied by $\pm 5\%$ and $\pm 20\%$ from its default value for $W^+W^- \to q\overline{q}q\overline{q}$ and $W^+W^- \to q\overline{q}\ell\overline{\nu}_\ell$ events, respectively, where the allowed ranges are taken from [39].

4.4.3 Four-fermion Background Modelling

This systematic uncertainty is estimated by using the KandY generator as an alternative to the default (KORALW) to simulate the WW-like four-fermion events, with the change in the measured multiplicity or R_N value assigned as the uncertainty. Note that owing to the $O(\alpha)$ corrections in KandY, the alternative WW-like four-fermion cross-section is 2.5% lower than that of KORALW, and so the same 2.5% reduction is also applied to the cross-section of the KORALW W^+W^- events when carrying out this test.

4.4.4 Z^0Z^0 Rate

An uncertainty is assigned to the assumed cross-section for ZZ events. It is estimated by varying the ZZ component of the four-fermion background by $\pm 11\%$ for $W^+W^- \to q\overline{q}q\overline{q}$ events [40], and $\pm 20\%$ for $W^+W^- \to q\overline{q}\ell\overline{\nu}_\ell$ events [39].

4.4.5 Residual Backgrounds

Two further small sources of background are considered. The first small source of background is only relevant for $W^+W^- \to q\overline{q}\ell\overline{\nu}_\ell$ events and so is considered for the multiplicity analysis alone. It is assigned as the effect observed on the measurements when all predicted $e^+e^- \to \ell^+\ell^-$ backgrounds are neglected.

The second source is due to two-photon background, and is estimated as the difference found in the final result when the small, predicted background from this source is included (default) or neglected.

4.5 Unfolding Method

For the multiplicity analysis, the results of the x_p and direct multiplicity analyses are compared and the difference in their central values is assigned as a source of possible uncertainty.

4.6 Centre-of-Mass Energy Dependence

The multiplicity and particle flow measurements are assumed to be independent of $\sqrt{s}$, as discussed in Section 3. An alternative choice considered for the particle flow analysis was to correct the measurements of R_N according to the weak energy dependence predicted by the KORALW model with JETSET hadronisation. The difference between these two assumptions is found to be small, at a level of 2% of the statistical uncertainty on the combined result, and is therefore neglected.

4.7 Cross-Check Using $\mathrm{W^+W^-} \to \mathrm{q\overline{q}}\ell\overline{\nu}_\ell$ Data

By way of a cross-check that the data are adequately described by the conventional hadronisation models, the particle flow analysis is repeated using $\mathrm{W^+W^-} \to \mathrm{q\overline{q}}\ell\overline{\nu}_\ell$ events, in which there can be no (inter-W) colour reconnection. The event selection is restricted to events in which the charged lepton is classified as either an electron or a muon. The four planes used in these events are defined by the jet or fermion directions derived from a kinematic fit in which the constraints of energy and momentum conservation are imposed (4-C fit, as in [20]). Figure 8(a) shows the distribution of particle flow for all $\mathrm{W^+W^-} \to \mathrm{q\overline{q}}\ell\overline{\nu}_\ell$ data, which are found to be described well by the predictions of the JETSET, HERWIG, ARIADNE and old JETSET models.

By construction, the two jet axes corresponding to the hadronically decaying W boson are centred at $\chi = 0$ and $\chi = 1$, while the direction of the charged lepton and that inferred for the unobserved neutrino are at $\chi = 2$ and $\chi = 3$, respectively. Note that charged particles associated with the leptonically decaying W bosons are not included in these figures. The non-zero multiplicity in the region between the two leptonic "jets" is due to the particles projected into this plane from the hadronically decaying W. Similarly, the abrupt change in the distribution in the region of the leptonic W is because none of the charged particles projected onto this plane plays a direct role in defining it.

Figure 8(b) shows the energy evolution of R_N for $\mathrm{W^+W^-} \to \mathrm{q\overline{q}}\ell\overline{\nu}_\ell$ events, together with the predictions of the same set of four hadronisation models. Similarly, the models provide a reasonable description of the data, giving confidence to the analysis procedure. No additional systematic uncertainty is assigned as a result of this study.

5 Results and Discussion

The measurements of the mean charged particle multiplicities corrected to the hadron level and averaged over the range $\sqrt{s} \simeq 189$–209 GeV, are:

$$\begin{aligned} \langle n_{\mathrm{ch}}^{\mathrm{4q}} \rangle &= 38.74 \pm 0.12 \pm 0.26 \ , \\ \langle n_{\mathrm{ch}}^{\mathrm{qq}\ell\nu} \rangle &= 19.39 \pm 0.11 \pm 0.09 \ , \\ \Delta\langle n_{\mathrm{ch}} \rangle &= -0.04 \pm 0.25 \pm 0.17 \ , \end{aligned}$$

where in each case the first uncertainty is statistical and the second systematic. The difference in mean charged particle multiplicities in hadronic W decays in $q\overline{q}q\overline{q}$ and $q\overline{q}\ell\overline{\nu}_\ell$ events, $\Delta\langle n_{\rm ch}\rangle$, is found to be consistent with zero within uncertainties. All models considered are found to lie within 1.2 standard deviations of the measurement, as shown in Table 2. As no evidence is found in this measurement for colour reconnection between the two hadronically decaying W bosons, the average of data from $W^+W^- \to q\overline{q}q\overline{q}$ and $W^+W^- \to q\overline{q}\ell\overline{\nu}_\ell$ events, weighted by statistical uncertainties and taking into account correlations in the systematic uncertainties, is used to yield a measurement of the charged particle multiplicity from a single hadronically decaying W,

$$\langle n_{\rm ch}^{\rm qq}\rangle = 19.38 \pm 0.05(\text{stat.}) \pm 0.08(\text{syst.}) \ .$$

As this average is made under the assumption that there is no colour reconnection between W bosons, the CR contribution to the W^+W^- hadronisation uncertainty has been removed.

The analysis of particle flow allows a simple comparison with models of colour reconnection, using the data of Table 5. The measurement obtained using approximately 625 pb^{-1} of data in the range 189–209 GeV yields:

$$R_N = 1.243 \pm 0.025(\text{stat.}) \pm 0.023(\text{syst.}) \ . \tag{2}$$

This result may be compared with the predictions of the models at $\sqrt{s}$=199.5 GeV given in Table 2. It can be seen that R_N measured in data is lower than all models except the SK-I ($k_I = 100$) sample. The (signed) significance of these differences is also presented, varying from approximately 4.4 standard deviations of the total error ($\sigma_{R_N}^{\rm total}$) for an extreme scenario of the SK-I model, to $-2.0\sigma_{R_N}^{\rm total}$ for HERWIG, with most other models populating a region around $-1\sigma_{R_N}^{\rm total}$.

Comparing the measured R_N with the predictions of Table 2, the data are seen to be closest to the predictions of the SK-I model with strength parameter $k_I = 0.9$. As this parameter is arbitrary, it may be varied to optimise the consistency with the measured R_N of Equation 2. The $\Delta\chi^2$ curve corresponding to this variation is presented in Figure 9. Parametrising this curve using a fourth order polynomial, the best agreement with data is obtained when approximately 37% of events are reconnected in the SK-I model, corresponding to the value $k_I = 1.0$. The 68% confidence level allowed region deduced from the $\Delta\chi^2$ curve corresponds to $0.10 < P^{\rm reco} < 0.56$. This result is not combined with the analysis of inclusive particle multiplicity as they have correlated systematic uncertainties and no significant improvement in sensitivity is expected.

It should be noted that the properties of the SK-I model vary significantly with the parton shower cut-off parameter and therefore this k_I cannot be directly compared to similar results from other LEP collaborations. Any combination of results from the different experiments is best performed on the basis of analysis of a common set of simulated events, analysed independently by each experimental collaboration [18].

6 Conclusions

The predictions of models of colour reconnection implemented within the ARIADNE Monte Carlo, the HERWIG model and the SK model, have been compared with OPAL data recorded at $\sqrt{s} \simeq$189–209 GeV using both inclusive measurements of particle multiplicity and a generalisation of the "string effect" analysis to the four-jet topology of $W^+W^- \to q\overline{q}q\overline{q}$ events.

Studies of reconnection phenomena using the extreme scenarios of the SK-I model show that changes up to approximately 1% may be expected in $\langle n_{\rm ch}^{\rm 4q}\rangle$, where the total experimental uncertainty

on measurements of $\langle n_{\rm ch}^{\rm 4q} \rangle$ is 0.7%. Other models predict somewhat smaller effects. Defining $\Delta\langle n_{\rm ch} \rangle$ using data alone provides a model-independent (but less sensitive) test of possible reconnection effects. The inclusive measurements of particle multiplicity find no evidence for such effects.

Measurements of particle flow in the OPAL data exclude an extreme scenario of the SK-I model and are compatible with other CR models such as SK-II, SK-II′, AR-2 and that of HERWIG. They are also compatible with models which do not include colour reconnection, slightly disfavouring the conventional HERWIG model. The results of this analysis are not combined with measurements of inclusive particle multiplicity as they have correlated systematic uncertainties and no significant improvement in sensitivity is expected. The best agreement with data is obtained using the SK-I model with a reconnection probability, $P^{\rm reco}$, of approximately 37%, corresponding to a model parameter $k_I = 1.0$ within the context of the OPAL tuning of the JETSET hadronisation model. The 68% confidence level allowed region deduced from the χ^2 curve corresponds to $0.10 < P^{\rm reco} < 0.56$. This result is used to help constrain the systematic uncertainty related to colour reconnection in measurements of the W boson mass [20].

Acknowledgements

We particularly wish to thank the SL Division for the efficient operation of the LEP accelerator at all energies and for their close cooperation with our experimental group. In addition to the support staff at our own institutions we are pleased to acknowledge the
Department of Energy, USA,
National Science Foundation, USA,
Particle Physics and Astronomy Research Council, UK,
Natural Sciences and Engineering Research Council, Canada,
Israel Science Foundation, administered by the Israel Academy of Science and Humanities,
Benoziyo Center for High Energy Physics,
Japanese Ministry of Education, Culture, Sports, Science and Technology (MEXT) and a grant under the MEXT International Science Research Program,
Japanese Society for the Promotion of Science (JSPS),
German Israeli Bi-national Science Foundation (GIF),
Bundesministerium für Bildung und Forschung, Germany,
National Research Council of Canada,
Hungarian Foundation for Scientific Research, OTKA T-038240, and T-042864,
The NWO/NATO Fund for Scientific Research, the Netherlands.

References

[1] G. Gustafson, U. Pettersson and P.M. Zerwas, Phys. Lett. **B209** (1988) 90.

[2] T. Sjöstrand and V.A. Khoze, Z. Phys. **C62** (1994) 281; Phys. Rev. Lett. **72** (1994) 28.

[3] T. Sjöstrand, Comput. Phys. Commun. **135** (2001) 238.

[4] G. Gustafson, J. Häkkinen, Z. Phys. **C64** (1994) 659;
C. Friberg, G. Gustafson and J. Häkkinen, Nucl. Phys. **B490** (1997) 289.

[5] L. Lönnblad, Z. Phys. **C70** (1996) 107.

[6] L. Lönnblad, Comput. Phys. Commun. **71** (1992) 15.

[7] Proceedings of CERN LEP2 Workshop, CERN 96-01, Vol. 2, p. 159,
eds. G. Altarelli, T. Sjöstrand and F. Zwirner, February 1996.

[8] G. Corcella *et al.*, J. High Energy Phys. JHEP 01 (2001) 010.

[9] J. Ellis and K. Geiger, Phys. Rev. **D54** (1996) 1967.

[10] K. Geiger, Comput. Phys. Commun. **104** (1997) 70.

[11] OPAL Collaboration, K. Ackerstaff *et al.*, Eur. Phys. J. **C1** (1998) 395.

[12] OPAL Collaboration, G. Abbiendi *et al.*, Phys. Lett. **B453** (1999) 153.

[13] DELPHI Collaboration, P. Abreu *et al.*, Eur. Phys. J. **C18** (2000) 203.

[14] Proceedings of CERN LEP2 Workshop, CERN 96-01, Vol. 1, p. 191,
eds. G. Altarelli, T. Sjöstrand and F. Zwirner, February 1996.

[15] A. Ballestrero *et al.*, J. Phys. G: Nucl. Part. Phys. **24** (1998) 365.

[16] D. Duchesneau, *New method based on energy and particle flow in* $e^+e^- \to W^+W^- \to$ *hadron events for color reconnection studies*, LAPP-EXP-2000-02,
`http://wwwlapp.in2p3.fr/preplapp/LAPP_EX2000_04.pdf`.

[17] JADE Collaboration, W. Bartel *et al.*, Phys. Lett. **B101** (1981) 129.

[18] The LEP Collaborations ALEPH, DELPHI, L3, OPAL, the LEP Electroweak Working Group, and the SLD Electroweak and Heavy Flavour Groups, *A combination of preliminary electroweak measurements and constraints on the Standard Model*, CERN-EP/2004-069, hep-ex/0412015.

[19] OPAL Collaboration, K. Ahmet *et al.*, Nucl. Instr. Meth. **A305** (1991) 275;
B.E. Anderson *et al.*, IEEE Transactions on Nuclear Science, **41** (1994) 845;
S. Anderson *et al.*, Nucl. Instr. Meth. **A403** (1998) 326.

[20] OPAL Collaboration, G. Abbiendi *et al.*, Eur. Phys. J. **Cnnn** (2005) mmm. *Completed OPAL* $M_{\rm W}$ *paper, to be sent to EPJ C at same time as this paper.*

[21] J. Allison *et al.*, Nucl. Instr. Meth. **A317** (1992) 47.

[22] T. Sjöstrand and V.A. Khoze, Eur. Phys. J. **C6** (1999) 271.

[23] S. Jadach *et al.*, Comput. Phys. Commun. **119** (1999) 272.

[24] OPAL Collaboration, G. Alexander *et al.*, Z. Phys. **C69** (1996) 543.

[25] OPAL Collaboration, G. Abbiendi *et al.*, Eur. Phys. J. **C35** (2004) 293.

[26] L. Lönnblad, private communication.

[27] OPAL Collaboration, G. Abbiendi *et al.*, Phys. Lett. **B507** (2001) 29.

[28] L. Lönnblad and T. Sjöstrand, Eur. Phys. J. **C2** (1998) 165.

[29] S. Jadach, B.F.L. Ward and Z. Was, Phys. Lett. **B449** (1999) 97;
S. Jadach, B.F.L. Ward and Z. Was, Comput. Phys. Commun. **130** (2000) 260.

[30] R. Engel and J. Ranft, Phys. Rev. **D54** (1996) 4244;
R. Engel, Z. Phys. **C66** (1995) 203.

[31] J. Fujimoto *et al.*, Comput. Phys. Commun. **100** (1997) 128.

[32] S. Jadach *et al.*, Comput. Phys. Commun. **140** (2001) 475.

[33] S. Jadach *et al.*, Phys. Lett. **B417** (1998) 326. S. Jadach *et al.*, Comput. Phys. Commun. **140** (2001) 432.

[34] OPAL Collaboration, G. Alexander *et al.*, Z. Phys. **C72** (1996) 191.

[35] N. Brown and W.J. Stirling, Phys. Lett. **B252** (1990) 657;
S. Catani *et al.*, Phys. Lett. **B269** (1991) 432;
S. Bethke, Z. Kunszt, D. Soper and W.J. Stirling, Nucl. Phys. **B370** (1992) 310;
N. Brown and W.J. Stirling, Z. Phys. **C53** (1992) 629.

[36] DELPHI Collaboration, P. Abreu *et al.*, Phys. Lett. **B401** (1997) 181;
OPAL Collaboration, G. Abbiendi *et al.*, Eur. Phys. J. **C8** (1999) 559;
ALEPH Collaboration, R. Barate *et al.*, Phys. Lett. **B478** (2000) 50.

[37] L3 Collaboration, M. Acciarri *et al.*, Phys. Lett. **B493** (2000) 233;
L3 Collaboration, P. Achard *et al.*, Phys. Lett. **B547** (2002) 139;
ALEPH Collaboration, S. Schael *et al.*, Phys. Lett. **B606** (2005) 265.

[38] OPAL Collaboration, G. Abbiendi *et al.*, Eur. Phys. J. **C36** (2004) 297.

[39] OPAL Collaboration, G. Abbiendi *et al.*, Phys. Lett. **B493** (2000) 249.

[40] OPAL Collaboration, G. Abbiendi *et al.*, Eur. Phys. J. **C32** (2003) 303.

Multiplicity	$\langle n_{\rm ch}^{\rm 4q}\rangle$	$\langle n_{\rm ch}^{\rm qq\ell\nu}\rangle$	$\Delta\langle n_{\rm ch}\rangle$	$\langle n_{\rm ch}^{\rm qq}\rangle$
Data	38.74	19.39	-0.04	19.38
Stat. error	0.12	0.11	0.25	0.05
Systematics				
$\rm W^+W^-$ hadronisation	0.22	0.08	0.08	0.06
BEC	0.03	0.01	0.05	0.01
Track definition	0.09	0.03	0.09	0.04
$\rm e^+e^- \to q\overline{q}$ modelling	0.11	0.01	0.10	0.04
$\rm e^+e^- \to q\overline{q}$ rate	0.01	0.00	0.02	0.01
Four-fermion background modelling	0.01	0.02	0.02	0.01
$\rm Z^0Z^0$ rate	0.01	0.01	0.02	0.00
Residual backgrounds	0.00	0.01	0.02	0.00
Unfolding procedure	0.00	0.01	0.02	0.00
Total syst.	0.26	0.09	0.17	0.08

Table 1: Results and estimated systematic effects in inclusive charged particle multiplicity measurements, see text for details.

Sample	$\Delta\langle n_{\rm ch}\rangle$	significance($\Delta\langle n_{\rm ch}\rangle$)	R_N	significance(R_N)
Data	-0.04 ± 0.30		1.243 ± 0.034	
SK-I($k_I = 100$)	-0.42	$+1.2$	1.092	$+4.4$
SK-I($k_I = 0.9$)	-0.29	$+0.8$	1.246	-0.1
SK-II	-0.14	$+0.3$	1.273	-0.9
SK-II′	-0.16	$+0.4$	1.277	-1.0
AR-2	-0.19	$+0.5$	1.271	-0.8
HERWIG-CR	$+0.32$	-1.2	1.282	-1.2
JETSET	-0.04	0.0	1.291	-1.4
HERWIG	$+0.02$	-0.2	1.311	-2.0
ARIADNE	$+0.02$	-0.2	1.286	-1.3
Old JETSET	-0.03	0.0	1.280	-1.1
AR-1	0.00	-0.2	1.304	-1.8

Table 2: Comparison of the average measured $\Delta\langle n_{\rm ch}\rangle$ and R_N in data with various models at $\sqrt{s} = 199.5$ GeV. The level of agreement in R_N is given by the significance(R_N), *i.e.*, $(R_N(\text{data}) - R_N(\text{model}))/\sigma^{\rm total}_{R_N}$, the difference between the average value of R_N in data and each model divided by the total uncertainty, and similarly for $\Delta\langle n_{\rm ch}\rangle$.

$\langle\sqrt{s}\rangle$ (GeV)	$\int \mathcal{L}dt$ (pb^{-1})	Selected events	Efficiency (%)	Purity (%)	Correct jet pairing (%)
188.6	183.0	675	39.7	86.1	90.3
191.6	29.3	92	39.1	86.5	90.0
195.5	76.4	277	40.0	87.1	89.9
199.5	76.6	253	38.9	87.0	89.4
201.6	37.7	145	38.4	84.2	89.1
206.0	220.5	757	37.7	86.2	88.5

Table 3: Summary of the integrated luminosity and number of candidate events used in the particle flow analysis, after all selection criteria, at each centre-of-mass energy in the range 189-209 GeV. The efficiency and purity are defined relative to the $\rm W^+W^- \to q\overline{q}q\overline{q}$ production process. The "correct" pairing in the rightmost column is defined by whichever association of observed jets in the detector minimises the sum of angular differences relative to the original four fermions from the $\rm W^+W^-$ decay.

Model	P^{reco} (%)	$\Delta R_N/\sigma^{\mathrm{stat.}}_{R_N}$
SK-I($k_I = 100$)	98.2	7.9
SK-I($k_I = 0.9$)	34.3	1.7
SK-II	17.2	0.6
SK-II′	16.1	0.5
AR-2	49.4	1.3
HERWIG-CR	23.0	0.9

Table 4: Summary of the predicted statistical sensitivity of the particle flow analysis for different models of colour reconnection at $\sqrt{s} = 199.5$ GeV. The sensitivity is defined as the difference between a given reconnection model and its corresponding "no reconnection" sample (ΔR_N), divided by the expected error of all data combined ($\sigma^{\mathrm{stat.}}_{R_N}$). P^{reco} is the fraction of colour reconnected events in each model. For AR-2, the no-CR model is AR-1.

Particle Flow	R_N
Data	1.243
Stat. error	0.025
Systematics	
$\mathrm{W^+W^-}$ hadronisation	0.015
BEC	0.002
Track definition	0.014
$\mathrm{e^+e^-} \to \mathrm{q\overline{q}}$ modelling	0.010
$\mathrm{e^+e^-} \to \mathrm{q\overline{q}}$ rate	0.002
Four-fermion background modelling	0.002
$\mathrm{Z^0Z^0}$ rate	0.001
Residual backgrounds	0.000
Total syst.	0.023

Table 5: Result and estimated systematic effects in particle flow measurements, see text for details.

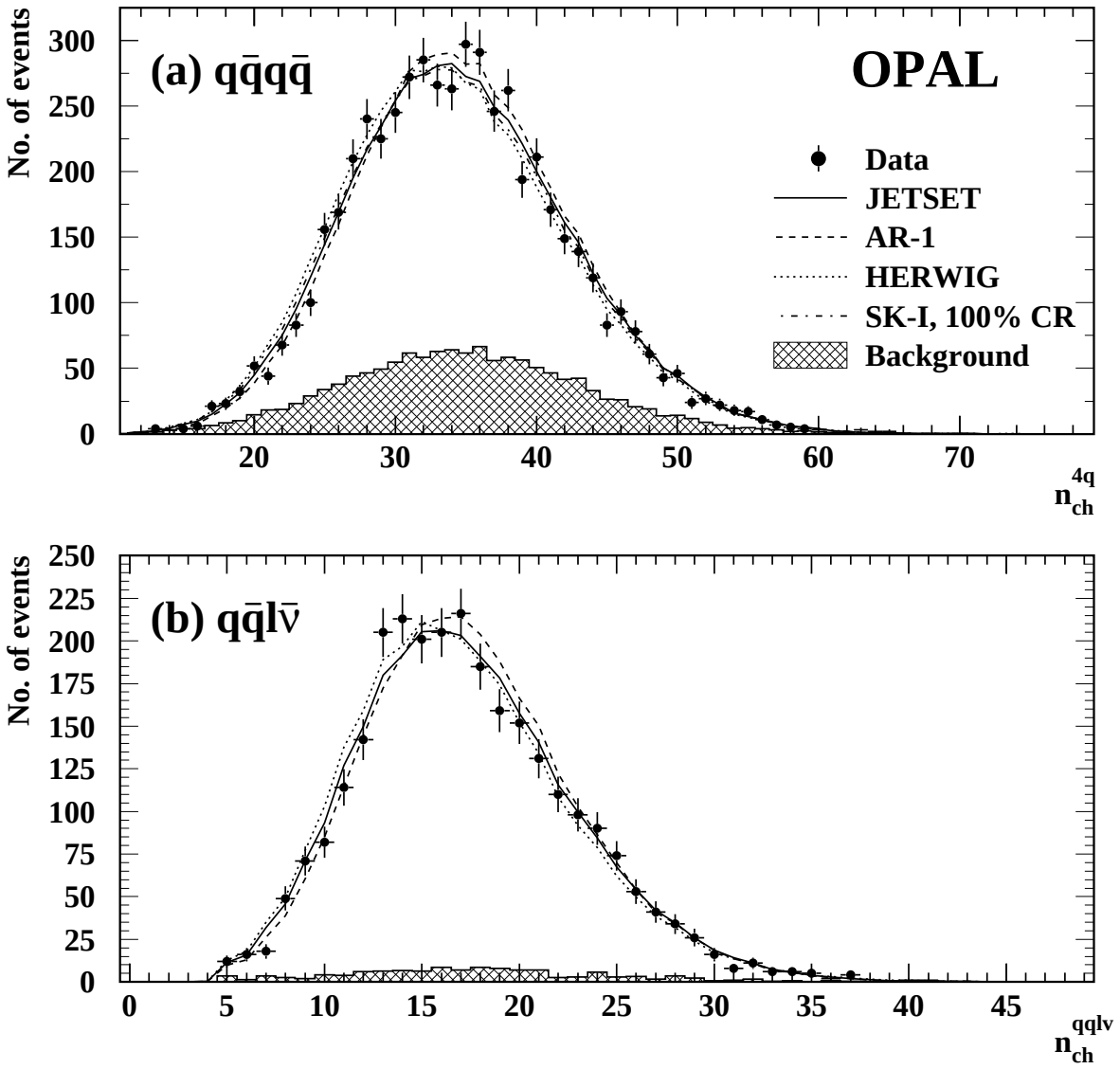

Figure 1: Uncorrected charged particle multiplicity distributions for data in the range $\sqrt{s}$=189–209 GeV: (a) $W^+W^- \to q\overline{q}q\overline{q}$ events and (b) the hadronic part of $W^+W^- \to q\overline{q}\ell\overline{\nu}_\ell$ events. Points indicate the data with statistical errors, lines show the expected sum of signal and background contributions for a variety of signal models, and the hatched histogram shows the expected background. Predictions of the conventional QCD hadronisation models JETSET and HERWIG, the AR-1 model and the 100% CR SK-I model, are shown.

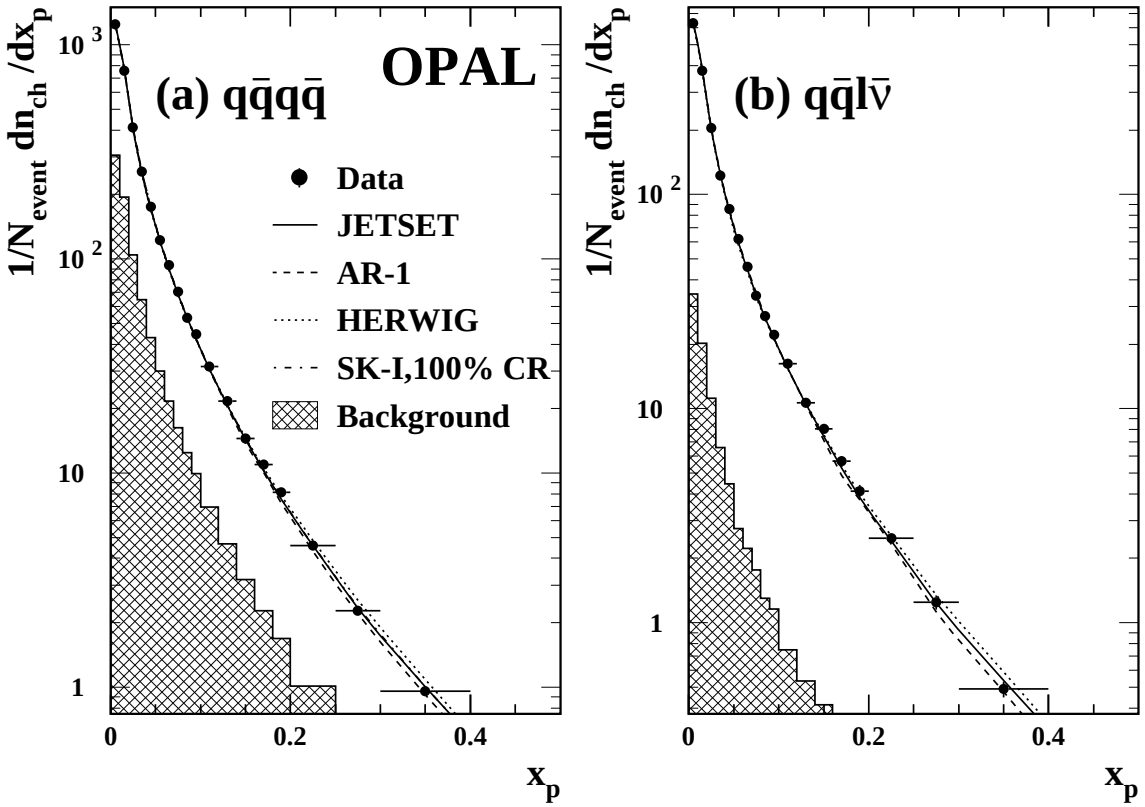

Figure 2: Uncorrected x_p distributions for data in the range $\sqrt{s}$=189–209 GeV: (a) $W^+W^- \to q\overline{q}q\overline{q}$ events and (b) the hadronic part of $W^+W^- \to q\overline{q}\ell\overline{\nu}_\ell$ events. Points indicate the data with statistical errors, smooth curves show the expected sum of signal and background contributions for a variety of signal models, and the hatched region shows the expected background. Predictions of the conventional QCD hadronisation models JETSET and HERWIG, the AR-1 model and the 100% CR SK-I model, are shown. Monte Carlo samples are normalised to the predicted number of signal plus background events, therefore the hatched regions correspond to the mean number of particles in candidate W^+W^- events which originate from background sources, rather than the mean number of particles per background event.

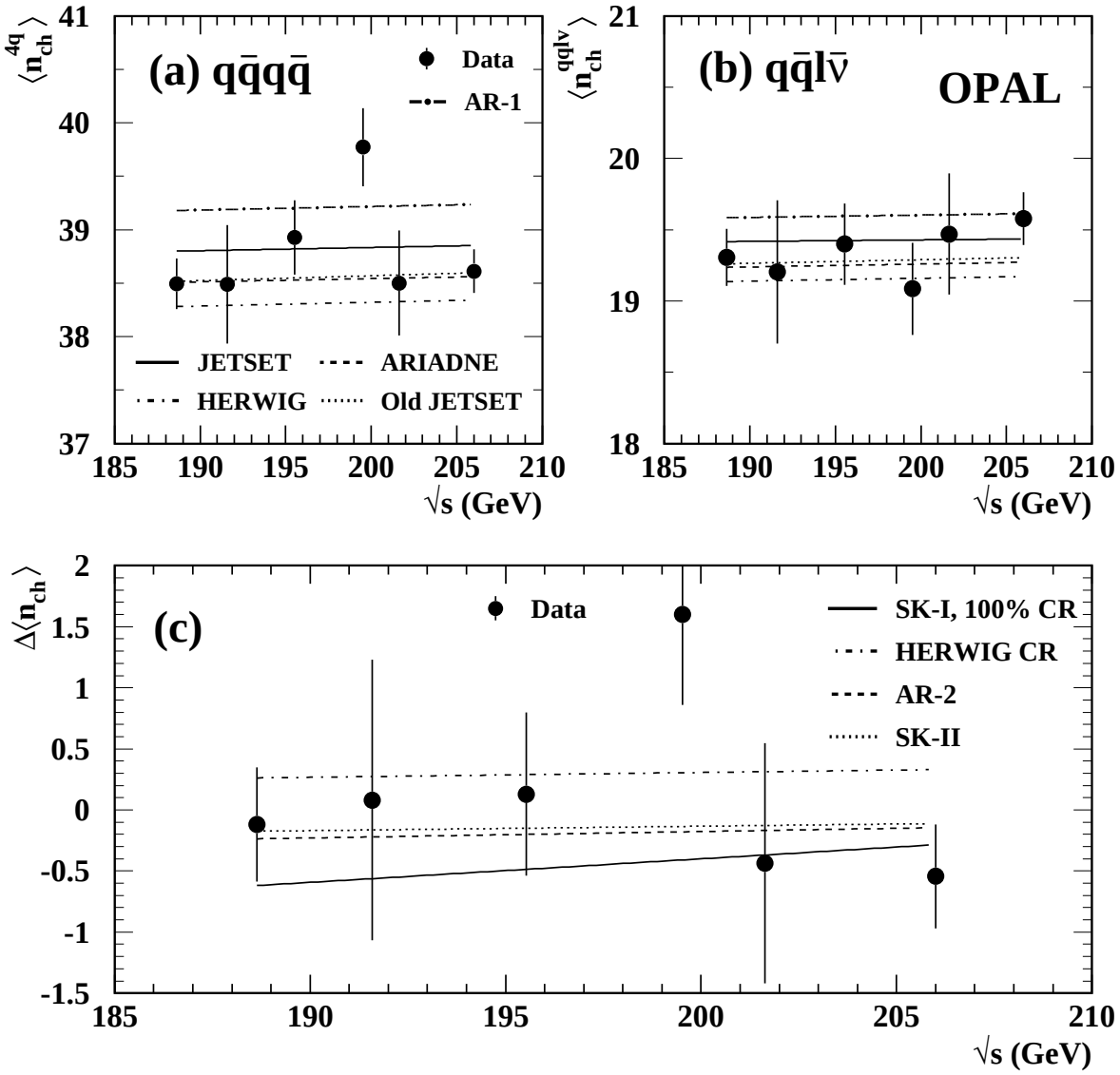

Figure 3: Centre-of-mass energy dependence of the measured (unfolded) mean charged particle multiplicity for (a) $W^+W^- \to q\overline{q}q\overline{q}$ events, (b) $W^+W^- \to q\overline{q}\ell\overline{\nu}_\ell$ events, and (c) the difference, $\Delta\langle n_{\rm ch}\rangle = \langle n_{\rm ch}^{4q}\rangle - 2\langle n_{\rm ch}^{qq\ell\nu}\rangle$. Points indicate the data with statistical errors and lines the predictions of W^+W^- models incorporating either conventional QCD hadronisation or CR. The predictions of JETSET, HERWIG, ARIADNE, the old tune of JETSET and AR-1 are indistinguishable from zero in (c), in all cases having values smaller in magnitude than 0.05, and so are not shown.

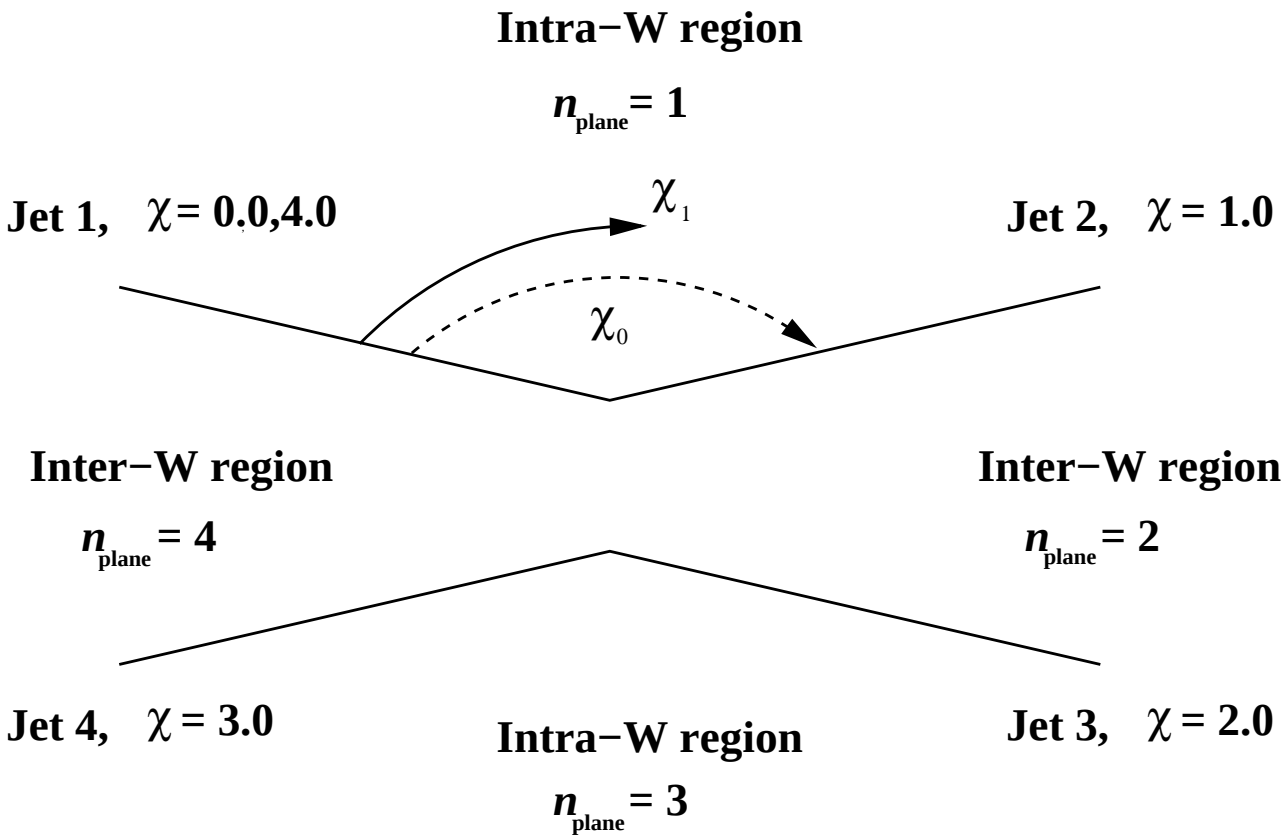

Figure 4: Illustration of inter-W and intra-W regions, and numbering convention adopted, as described in Section 3.

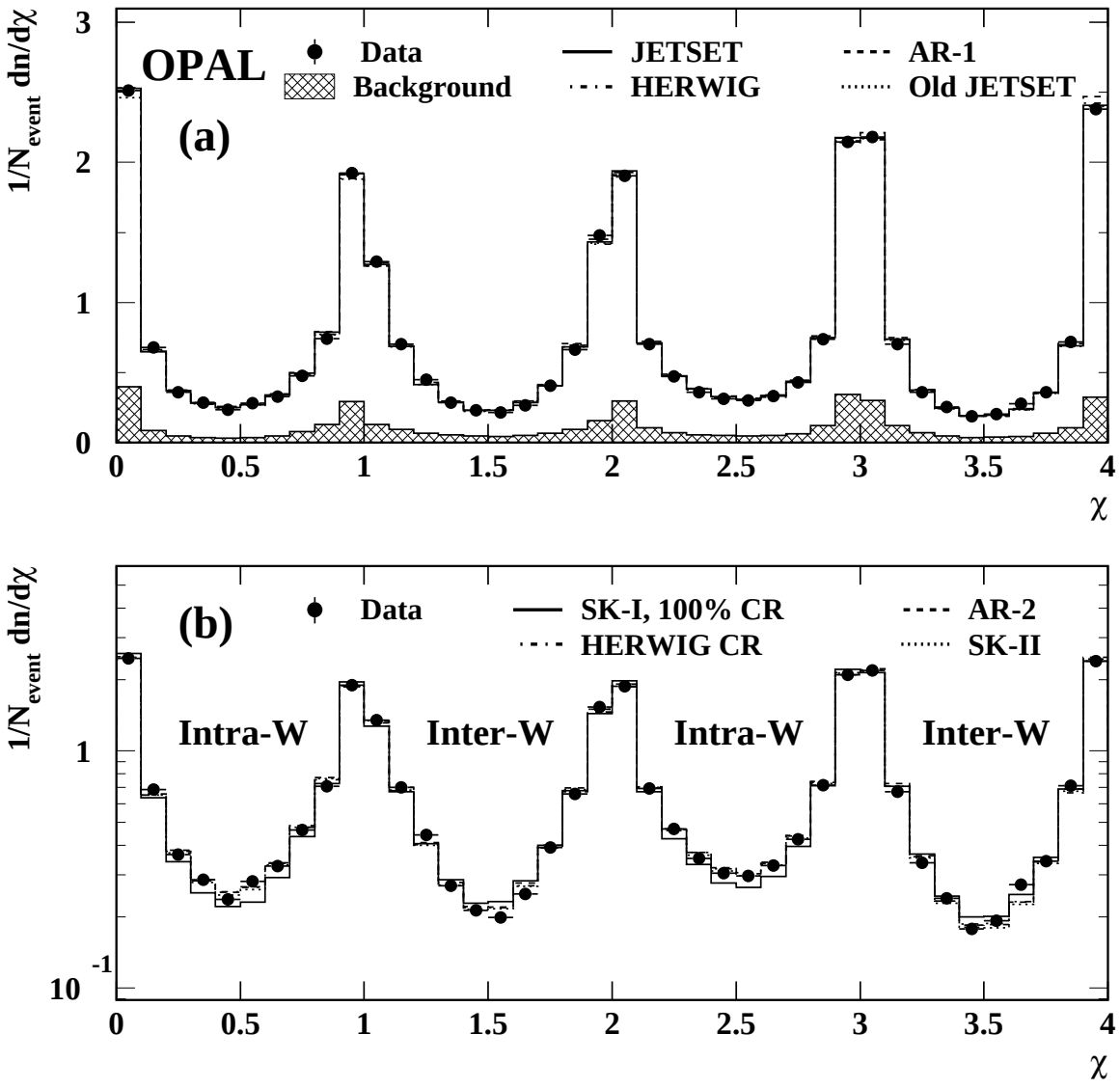

Figure 5: The particle flow distribution in the four inter-jet planes, normalised event-by-event to the inter-jet angles, as described in the text and in Figure 4. Points represent the data with statistical errors. (a) compares the data with the predictions of conventional QCD hadronisation Monte Carlo models and AR-1, (b) compares the data, after background subtraction, with several CR models. Monte Carlo samples are normalised to the predicted number of signal plus background events, therefore the hatched region in (a) corresponds to the mean number of particles in candidate $W^+W^- \to q\overline{q}q\overline{q}$ events which originate from background sources, rather than the mean number of particles per background event.

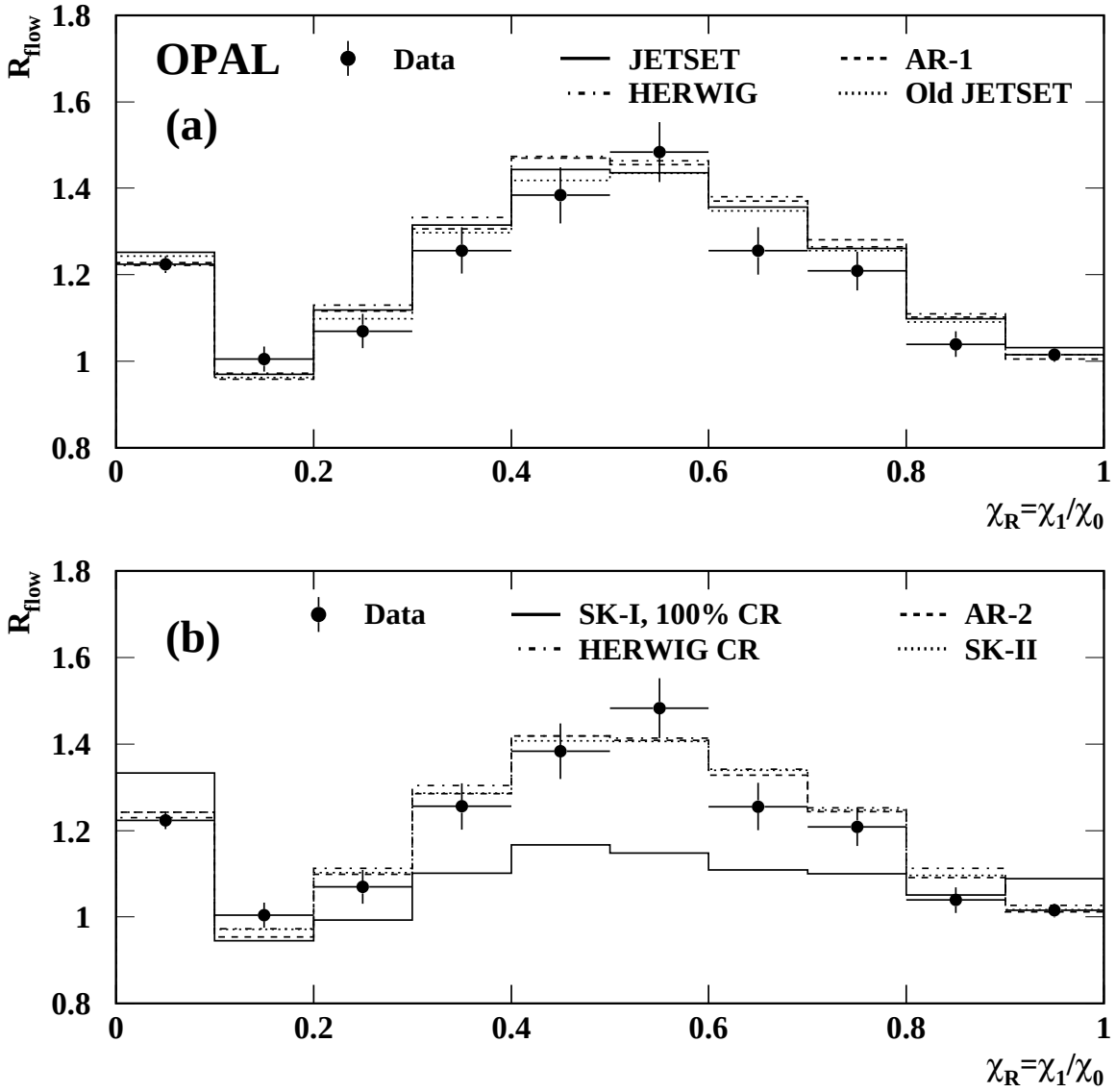

Figure 6: Distribution of $R_{\rm flow}$, the ratio of the particle flow in the intra-W regions to that in the inter-W regions. Points represent the data after background subtraction, with statistical errors. (a) compares the data with the predictions of conventional QCD hadronisation Monte Carlo models and AR-1, (b) compares the data with CR models. Note that there are correlations between bins in these distributions.

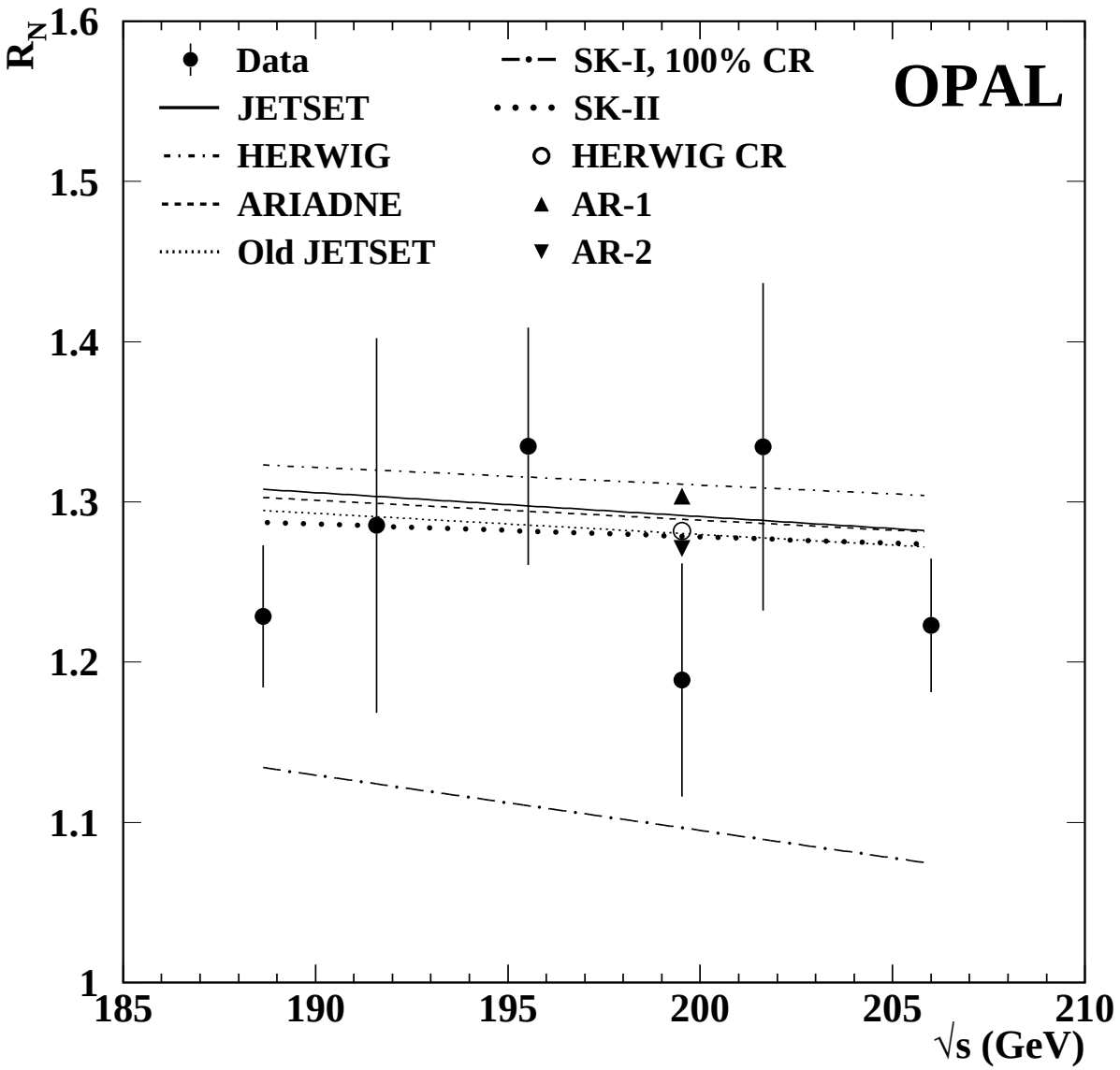

Figure 7: Centre-of-mass energy dependence of R_N for $W^+W^- \to q\overline{q}q\overline{q}$ events. Points indicate the data with statistical errors and lines the predictions of W^+W^- models incorporating either conventional QCD hadronisation or CR. The predictions of the HERWIG CR model, AR-1 and AR-2, which are only available at $\sqrt{s}$=199.5 GeV, are indicated by symbols.

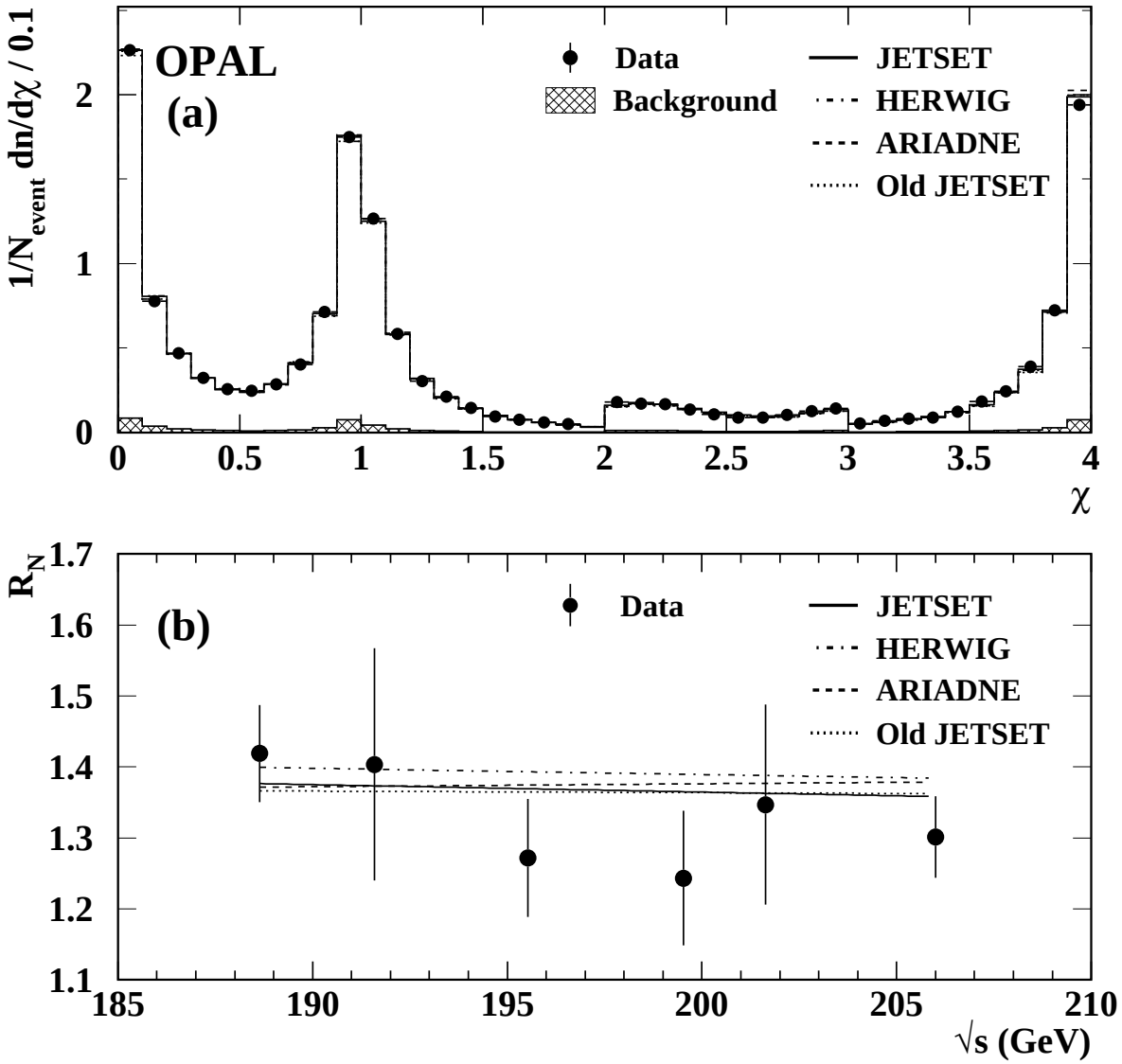

Figure 8: (a) The particle flow distribution (as in Figure 5) for $W^+W^- \to q\overline{q}\ell\overline{\nu}_\ell$ events and conventional QCD hadronisation Monte Carlo models, as described in Section 4.7. Points represent the data with statistical errors and the hatched region the sum of all background contributions. (b) The energy evolution of R_N as measured in $W^+W^- \to q\overline{q}\ell\overline{\nu}_\ell$ events, in comparison with the predictions of conventional QCD models.

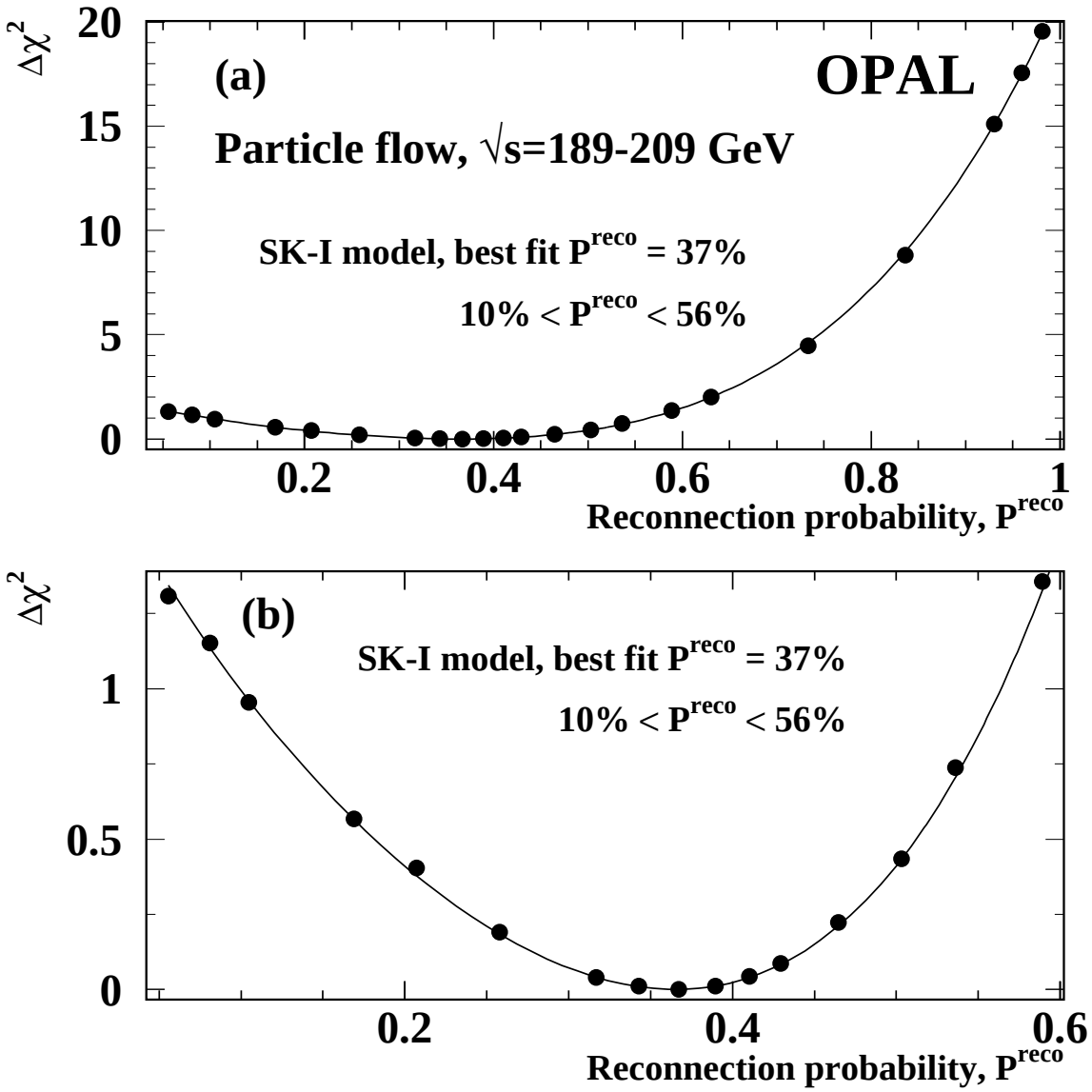

Figure 9: $\Delta\chi^2$ curve obtained from comparison of the average R_N measured using OPAL data between 189 GeV and 209 GeV, with the predictions of the SK-I model as a function of the fraction of reconnected events, $P^{\rm reco}$, carried out at a reference centre-of-mass energy of 199.5 GeV. (a) shows the entire range of $P^{\rm reco}$, while (b) shows the lower $P^{\rm reco}$ range of (a) in more detail. The best agreement between the model and data is obtained when 37% of events are reconnected in this model.